Combined Ion Conductance and Atomic Force Microscope for Fast Simultaneous Topographical and Surface Charge Imaging

Journal Article

Author(s):
Dorwling-Carter, Livie; Aramesh, Morteza; Han, Hana; Zambelli, Tomaso; Momotenko, Dmitry

Publication date:
2018-10-02

Permanent link:
https://doi.org/10.3929/ethz-b-000302117

Originally published in:
Analytical Chemistry 90(19), https://doi.org/10.1021/acs.analchem.8b02569

Funding acknowledgement:
174217 - Single Entities at High Magnification: Mapping, Measuring and Manipulating Nanoparticles (SNF)

Combined Ion Conductance and Atomic Force Microscope for Fast Simultaneous Topographical and Surface Charge Imaging

Livie Dorwling-Carter, Morteza Aramesh, Hana Han, Tomaso Zambelli and Dmitry Momotenko*

Laboratory of Biosensors and Bioelectronics, Institute for Biomedical Engineering, ETH Zurich, Zurich, CH-8092, Switzerland

KEYWORDS *AFM, microchanneled cantilever, FluidFM, surface charge, SICM, nanopipette*

ABSTRACT: We report here an advanced approach for simultaneous and independent sub-microscale imaging of local surface charge and topography using microchanneled cantilevers, also known as FluidFM nanopipette probes. These hollow cantilevers with a 300 nm opening are employed for ion current measurements that provide access to the local properties of the electrical double layer using the phenomenon of ion current rectification, while also taking advantage of the force sensing capabilities for accurate probe vertical positioning and topography imaging. The independent nature of this atomic force microscope (AFM) feedback opens up a possibility to significantly increase the sensitivity for probing local surface charges in a wider range of salt concentrations, especially in electrolytes of low ionic strength (below 10 mM), where classical local ion conductance measurements with glass nanopipettes would suffer from inaccuracies and instabilities, but where the electrical double layer extends further into the liquid medium and has stronger effect on the measured ion currents for charge imaging. We demonstrate that the measurements with FluidFM do not compromise the positioning accuracy and enable accurate and simultaneous topographical and charge imaging in contact mode (similar to AFM) at high scanning rates, approaching thousands of pixels per second, therefore overtaking state-of-the-art techniques for charge mapping by at least two orders of magnitude (the probes reach translation rates of 120 μm s^{-1} equating to 2 ms per image pixel). We also reveal experimentally the physical limit of this high speed scanning, constrained by the rate of ion redistribution in surface-induced rectification required for double layer sensing and charge mapping.

Surface charge influences phenomena at interfaces, where it determines numerous processes and equilibria, from ion adsorption[1] and colloidal stability,[2,3] to interactions between living systems and their environment.[2,4,5] In electrolyte solutions, those charges contribute to the existence of the so-called electrical double layer (EDL) at the sample-electrolyte interface, with counter-ions of electrolyte accumulating to compensate the charges at the interface. The capability to probe the double layer properties opens access to sensing local surface charges. Traditional techniques such as zeta potential measurements[6] or potentiometric titrations[7] aim to assess surface charges but do not offer the spatial resolution necessary to acquire information about charge distribution on heterogeneous materials and interfaces. Recently, the potential of scanning probe techniques, such as atomic force (AFM)[8–12] and scanning ion conductance microscopy (SICM)[13–16] has been extended for resolving local surface charge magnitudes at interfaces. In AFM measurements, the deflection of the cantilever is used to probe local forces that arise at the interface. However, these forces between the cantilever and the charged interface can have a rather different nature (not necessarily exclusively electrostatic), making the identification of the partial contribution of the double layer to the overall force measurement difficult. Additionally, the limited magnitude of these interfacial forces coupled with the small range of distance in which the probe is sensitive to surface charge (a few nanometers at the pre-contact with the sample) makes surface charge mapping with AFM further challenging. On the contrary, the purely non-contact nature of SICM measurements that rely on local ion sensing offers a high sensitivity to interfacial properties over a larger range of distances,[17] making SICM a powerful tool for local functional measurements.[18]

SICM uses a bias between an electrode in an electrolyte-filled glass pipette and an electrode in bulk solution to generate a distance-dependent ion current through the capillary orifice (typically ranging from several tens to hundreds of nanometers in diameter). As the probe is approached towards the sample, the resulting restricted flow of ions at the pipette tip leads to a noticeable increase in resistance (*i.e.* drop in current magnitude) that can be used to control the probe-sample distance and, therefore, allows to reconstruct the topography of the sample when the probe is scanned above the specimen.[13,19] Nonetheless, this ion current is not only a function of the tip-to-substrate distance but is also affected by the local conductivity at the probe opening, which can be influenced by the presence of the EDL. Whereas at high concentrations the limited thickness of the EDL justified negligible surface charge effects for purely topographical imaging, the increased Debye length at lower ionic strengths leads to surface charge effects that can no longer be neglected in the recorded current. This allows to extend SICM towards surface charge mapping[14–16,18,20–22] by exploiting the phenomenon of surface-induced ion current rectification (SIR), where the probe shows surface charge-dependent current amplitudes as a result of accumulation or depletion of ions at charged interfaces.[23,24] The magnitude of ion current rectification significantly depends on the electrolyte concentration and is amplified in diluted electrolytes from the

stronger influence of ion accumulation/depletion in conical nanopipettes.[25] Thus, SICM measurements in diluted electrolytes enable higher sensitivity for surface charge mapping but, at the same time, bring the challenge of decorrelating the variations in the ion current arising from the local topography and EDL heterogeneities. Several strategies have been developed to extract independent topographical and charge information from local ion current measurements. Some resort to alternating current (AC) components of the ion current, induced by either small harmonic modulation of the vertical position of the probe,[14] or by bias modulation where the AC phase shift at zero bias is used for vertical feedback, while the direct current (DC) recorded during a cyclic voltammogram at proximity to the surface is used for charge measurement.[20] Other strategies exploit the dependence of the SIR with the applied bias to identify surface charges by scanning under DC current feedback the same area at two opposite biases[16,23] while the true topography needs to be measured by a complementary AFM imaging.

Herein, we present a novel strategy to resolve simultaneously and independently the distributions of surface charge and topography by combining the capabilities of AFM and SICM in a single probe: the approach known as FluidFM, based on hollow AFM cantilevers,[17,26] which previously has demonstrated its capacity for fine topographical imaging using a compound ion current and force feedback. Here we extend functional imaging capabilities of this approach and employ the AFM force control of the FluidFM probe to resolve the topography of the sample in contact mode, while the simultaneously recorded current through the microfluidic cantilever is independently sensing the local ionic environment related to the EDL and surface charge. The success of this methodology is based on the advantages of two different physical principles – the bending of the cantilever for force measurement and the ion current variation associated with the changes in the EDL – to enable fast and simultaneous probe positioning and ion sensing. Furthermore, by relying on the forces for feedback control (instead of the current used in SICM), this strategy offers the possibility to perform surface charge mapping in lower electrolyte concentrations than in conventional SICM, where difficulties in vertical probe positioning associated with working with lower ion current amplitudes for feedback can arise. This provides higher charge mapping contrast due to the amplified ion current rectification (ICR) effects under low ionic strength conditions. Finally, FluidFM enables simultaneous topographical and charge imaging at higher acquisition rates than the state-of-the-art SICM strategies with two orders of magnitude speed improvement.

EXPERIMENTAL SECTION

Solutions

Electrolyte solutions were prepared in ultrapure Milli-Q water (Millipore Corp., resistivity ca. 18.2 MΩ at 25°C). The pH of all solutions was measured using a S20 SevenEasy™ pH meter (Mettler Toledo).

Substrates

Poly-D-Lysine. Poly-D-Lysine (PDL, P7280, Sigma-Aldrich, Switzerland) patterns were prepared using microcontact printing method, following a protocol adapted from Ricoult *et al.*[27] In brief, a polydimethylsiloxane (PDMS, Sylgard 184, Dow Corning) stamp was replicated from a patterned SU-8 mold. Prior to printing, the PDMS stamp was sonicated for 15 minutes in 70 % ethanol to remove surface contamination. An air plasma-cleaned glass coverslip was put onto the PDMS stamp to allow a droplet of inking solution to wet the sample for 5 minutes. The inking solution consisted of 100 µg/mL PDL and 25 µg/mL of Alexa Fluor 488 dye (Thermo Fisher Scientific) in PBS buffer. The stamp was then rinsed for 5 s sequentially in PBS and water and dried under flow of nitrogen before printing it on a freshly plasma-activated glass Willco dish (Willco Wells B.V., Netherlands).

Polystyrene. The polystyrene film on glass was prepared as described elsewhere.[14] Polystyrene beads (Sigma-Aldrich) were dissolved in chloroform (Sigma-Aldrich) to a final concentration of 0.66 mg/mL. A small glass coverslip was first sonicated in acetone for 10 minutes, then rinsed in Milli-Q water and sonicated in water for 10 minutes. After drying under nitrogen flow, the glass substrate was plasma cleaned for 2 minutes in oxygen plasma and directly immersed for 30 s into the 0.66 mg/mL polystyrene solution to form a thin film. After chloroform evaporation, the coverslip was fixed onto a Willco dish with UV-curable adhesive (Loctite 3311).

Glass. For the experiment comparing the approach curves on glass in different ion concentrations, the glass Willco dish substrate was oxygen plasma-cleaned for 10 min.

Probes

Commercially available FluidFM nanopipette probes (opening diameter 300 nm, stiffness of 2 N m^{-1}) were purchased from Cytosurge (Switzerland). Prior to filling, the probes were oxygen plasma-cleaned for 2 minutes to increase wettability of the microchannel.

Instrumentation

The FluidFM microscope (Cytosurge and Nanosurf AG, Switzerland) was adapted for ion conductance measurements. The setup was equipped with two Ag/AgCl quasi-reference counter electrodes, one inserted in the reservoir of the probe (connected to a Pico 2 USB-powered patch clamp amplifier, Tecella, USA) and another in the bulk solution (connected to the amplifier's ground). Voltage control was performed via the WinWCP software (University of Strathclyde, UK) while data was acquired with the C3000 control software of Nanosurf. All potentials values reported in this work refer to the potential at the electrode in the reservoir of the FluidFM probe with respect to the electrode in the bulk solution. Current-voltage curves were recorded using an Autolab Potentiostat (PGSTAT302N, MetroOhm).

Experimental procedures

Approach curves were recorded by moving automatically the probe towards the substrate with AFM force feedback at a speed of 500 nm/s and using a sampling rate of 2.3 kHz. The force feedback was used to identify the moment of contact of the probe with the substrate. The data were then low pass filtered (f_{cut}=60 Hz). To avoid the impact of the angle of the approach, the levelling of the sample and AFM head was kept the same within each experiment.

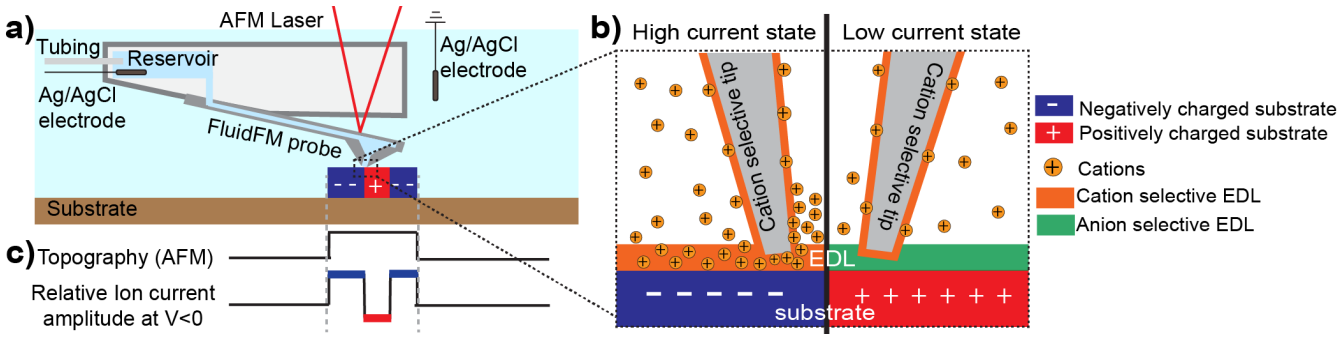

Figure 1. Principle of surface charge mapping with the FluidFM. a) Schematic representation of the FluidFM probe operating over a charged feature on the substrate. b) Illustration of the surface-induced rectification phenomenon occurring in the negatively charged and negatively biased nanopipette probe over a negatively charged (left) and a positively charged (right) substrate. c) Schematic line scan profiles depicting the AFM topography and ion current recorded in a configuration depicted in (a) with a negatively biased cantilever probe.

All images were acquired using raster scanning in AFM contact mode (force feedback on a setpoint, indicated for each experimental dataset). A time of 2-5 minutes was allowed after each change of bias and each contact with the substrate to enable probe current stabilization. All images consisted of 256 pixels/line while their imaging speed was adjusted.

RESULTS AND DISCUSSION

Working principle

FluidFM[26,28] is a recently developed force-controlled nanopipette that emerged from the combination of an atomic force microscope cantilever with an integrated microchannel for microfluidics: a hollow Si_3N_4 cantilever connects the probe aperture to an external liquid reservoir, allowing the probe to act as a force sensor and as a nanopipette. When equipped with electrodes (two quasi-reference counter electrodes, one in the probe reservoir and another one in the bulk solution) and electrochemical instrumentation, the FluidFM turns into a scanning ion conductance probe[17] (Figure 1a) capable to record local ion currents. In this work, a commercially available FluidFM probe with a 300 nm opening diameter was used. Also, cantilevers with smaller opening diameters can be readily fabricated.[17] In contrast to pulled capillaries, which could be fabricated only within certain geometrical limits (narrow range of possible inner/outer angles, almost exclusively round conical shapes *etc*), FluidFM probes produced using state-of-the-art microfabrication techniques offer a broader choice of geometrical arrangements, however, typically at a higher cost.

The electrical properties of the FluidFM probes are determined by the total resistance, which consists of the resistance of the microchannel that connects the liquid reservoir to the pyramidal tip and the tip resistance (see details in the Supporting Information section SI-1). In contrast to laser-pulled micro- and nanopipettes, where the electrical characteristics of the probe are determined almost exclusively by the dimensions of the pipette aperture and opening angle, FluidFM probes typically exhibit a resistance dominated by their microchannel[29] (~95.6% of the total probe resistance). As a result of the dimensions of the microchannel (1.5 mm × 30 µm × 1 µm), typical electrical resistances of the FluidFM probes approach 25 MΩ in 150 mM KCl and can be as high as 3 GΩ in 1 mM KCl solutions. At this scale of probe opening dimensions, this resistance is comparable to that of a glass nanopipette, however, upon the reduction of the probe size, FluidFM probes should exhibit significantly smaller impedance than pulled glass capillaries (*e.g.* around an order of magnitude lower when opening diameter drops to tens of nanometers scale), which can provide the FluidFM higher sensitivity to local ion sensing when using smaller probes.

Figure 1a depicts a typical imaging strategy using FluidFM probes. The AFM force feedback based on laser beam deflection from the cantilever is employed to resolve topographical features, illustrated as a topographical step on the substrate, in contact mode (intermittent contact techniques can also be used for positioning,[17] however, complex cantilever dynamics can become an issue in some cases). Independently from the force measurement, the concurrent recording of the ion flow through the orifice at the cantilever tip is used to probe the local ionic environment. Figure 1b depicts the charge sensing principle based on the phenomenon of surface-induced ion rectification[14,24] (SIR). SIR leads to accumulation or depletion of ions at charged interfaces that results in a probe current enhancement or diminution depending on the bias polarity as well as the sign and the magnitude of the surface charge. For instance, at negative biases a cation-selective tip, such as our negatively-charged FluidFM nanopipette (confirmed by voltammetric measurement in bulk solution, more details in Supporting Information SI-1), is recording higher currents on a negatively charged substrate (Figure 1b, left) due to the enhanced cation concentration within the probe-to-substrate gap and at the very tip of the pipette. Over a positively charged sample (Figure 1b, right), the sample surface carries an anion-selective EDL, which repels cations, which considerably reduces the cation flow into the probe, leading to a reduction in the recorded current within the nanopipette. It is therefore possible in a single scan with the FluidFM (in this case biased negatively) to resolve both the structure, *i.e.* sample topography by AFM, and functional information, such as surface charge related to the local EDL at the sample. This is schematically illustrated in Figure 1c, which depicts corresponding height data and ion current profiles over a feature that carries charge heterogeneities. Alternatively, a positive bias could be applied. In this case, ICR scenarios are inversed, with a more positive surface charge causing less efficient depletion of cations (higher current through the probe). Nonetheless, the higher sensitivity of the negatively charged FluidFM probe for cations privileges working at negative biases due to the increased current and contrast (Supporting Information SI-2).

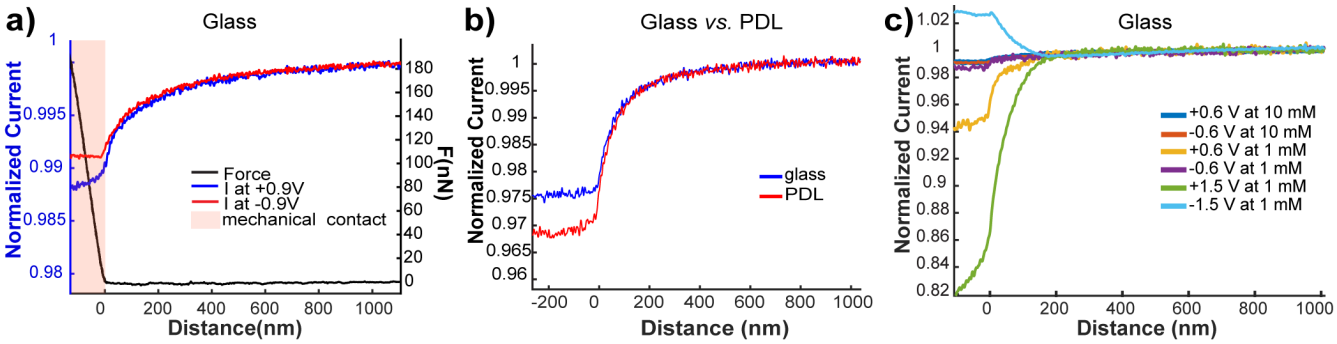

Figure 2. Probe approach curves. a) Approaches over the glass substrate in 10 mM KCl recorded at ±0.9 V (blue and red traces). The simultaneously acquired force-distance curve (black trace, see also the axis on the right of the graph) is used to identify the moment of contact with the substrate. The pink area indicates the working distance beyond the point of contact between the probe and the substrate, i.e. AFM contact mode. b) Approaches over the glass (blue) and PDL (red) in 10 mM KCl using a negatively biased (-0.25 V) FluidFM probe. c) Approach curves over the glass substrate in 10 mM and 1 mM KCl at different probe bias (±0.6 V and ±1.5 V). See the legend for details. All curves are normalized to the ion current value in the bulk. Note that the dark blue line thickness was increased for the clarity of representation

Electrical double layer sensing

Figure 2a demonstrates the influence of the tip bias on the current measured during the probe approach towards a glass substrate. Glass was chosen as an example of a negatively charged substrate, with known rectifying properties previously studied with glass nanopipettes.[14,25,30] In the approaches shown in Figure 2a, the simultaneously recorded AFM force-distance curve indicates the deflection of the cantilever and is used to detect the probe-to-substrate contact point. All current approach curves are normalized to the current in bulk, herein at distances above 1 µm. Both current-distance curves show a gradual drop of the current magnitude as the tip gets closer to the substrate due to the ion flow hindrance. At the point of mechanical contact (identified from the onset of a steep increase in the simultaneous forces), the current values vary depending on the bias polarity: at +0.9 V, the normalized current drops and settles at 0.991, whereas at -0.9 V the normalized current drops to 0.988, indicating the effect of SIR. Interestingly, the approach curves also show that despite increasing forces between the tip and the glass (here up to 180 nN), the current remains almost constant after the contact with the sample. The probe geometry with its four-peak apex and the intrinsic inclination angle (~10°) between the tip and the sample prevents the ion flow from complete blockade (see Supporting Information SI-1). As can also be expected, the magnitude of SIR is strongly distance-dependent. At probe-to-substrate separations exceeding 50 nm there is little to none difference between the approach curves, and the strongest SIR is observed after the probe-substrate contact point (region marked in pink in Figure 2a), where the distance between the cantilever opening and the substrate is the smallest and is determined by probe geometry, opening size and inclination angle. Typically, in our experimental arrangement, this gap where SIR takes place is in the range of 7 to 80 nm (see Supporting Information SI-1), close enough for the SIR to occur using the FluidFM probe with *ca.* 300 nm opening diameter. Thus, the FluidFM nanopipette benefits from the potential to achieve short working distances in contact mode that determines its sensitivity towards local EDL/charge sensing at interfaces.

Another important point to consider for FluidFM positioning is the mutual electrostatic repulsion or attraction that can potentially exist between the cantilever and the substrate, which further can compromise the precision of the topography tracking. Accurate cantilever landing requires appropriate force feedback setpoint (SP), adjusted to the cantilever stiffness. In our work, we did not observe any significant cantilever deflection due to repulsive or attractive forces near the contact point since these surface interactions are smaller than a few hundreds of pN,[11,12,31] which had no effect on our FluidFM probe (with stiffness around 2 N m^{-1}). Our choice of SP in the range of 3-5 nN ensured that the tip is engaged into contact with the sample and minimized the influence of electrostatic repulsion/attraction on the topography tracking. Also, these SP values were found to be optimal for reproducible imaging and minimal damage to the samples. Indeed, a more careful choice of SP would be required for imaging softer samples, where local deformation of the substrate might cause a variation of the probe current amplitude[17] and lead to difficulties with either probe positioning or interpretation of the ion current data.

Measurements of the ICR magnitudes at interfaces enable differentiation between substrates with different surface charges and charge polarities. As the next step, we patterned the glass substrate with regions each expected to exhibit either a positive or a negative charge: as such a system, we chose a negatively charged glass and a micro contact-printed poly-D-lysine (PDL), a positively charged polycation at pH=5.6, which readily adsorbs on glass. Figure 2b demonstrates the variation of the tip current occurring upon the approach on such a substrate at the fixed probe bias of -0.25 V. Approach curves demonstrate that at the identical negative probe potential, the tip current at the contact point differs for the two interfaces. The normalized current on PDL is around 0.969, which is 0.71% lower than on glass (0.976), indicating a different rectification behavior of the interfaces with ion current amplification on negatively charged (in this case glass) and diminution on positively charged (PDL) substrates under the experimental conditions herein. In contrast to other approaches[16,20,21] that require a different probe voltage for positioning and for charge measurement, the FluidFM is therefore capable to sense the variation of surface charges using a single bias value.

EDL sensing and mapping in diluted electrolytes

Several strategies can be envisioned to increase the contrast and sensitivity of nanopipette techniques towards surface charge.

The choice is typically between using smaller probes,[25] applying higher biases[20] or lowering the electrolyte concentration[32] to increase the effect of SIR. In the latter strategy, rectification is amplified both within the probe (we found a rectification ratio in 1 mM KCl approaching 12.3 as compared to 1.45 in 10 mM KCl, see Supporting Information SI-1) and at the charged surface, where ions accumulation extends further into the electrolyte solution. In our work, we take advantage of this approach to enhance significantly the sensitivity of our probes for charge sensing.

Figure 2c shows approach curves acquired over the glass substrate at various electrolyte concentrations and at different voltage biases. The approaches in 10 mM KCl at opposite biases (±0.6 V, red and dark blue lines) exhibit a rather small rectification (both currents settle at 0.991). In 1 mM electrolyte, the + 0.6 V (yellow) and – 0.6 V (violet) approaches are clearly distinguished, both at the contact (where the normalized current drops to 0.989 at -0.6 V *vs*. 0.938 at +0.6 V) and within 200 nm above the sample. This highlights the higher sensitivity of the ion current towards double layer effects at increased tip-to-substrate distances compared to 10 mM KCl (same biases applied). At higher voltage (-1.5 V, cyan line), the EDL current enhancement that arises from the accumulated charges on the glass interface dominates over the natural drop in current associated with current hindrance at close probe working distances. This leads to an interesting case where the probe current in contact reaches higher values than in the bulk (1.034 here). Interestingly, the ion current magnitude is prone to transient variation and drift at positive voltage (see green and yellow traces on Figure 2c) even after the probe is engaged with the substrate. This effect is likely to be related to the rate of ion redistribution, which depends on the initial ICR state, bias polarity and magnitude, as well as the speed and direction of rectification change[33] (refer to Supporting Information SI-3 on the reproducibility of those data). The higher contrast in diluted electrolytes is advantageous for mapping surface charges without the need of a significant reduction of the probe size, which can become important for mapping larger charge features or scanning larger areas. Furthermore, the force-controlled probe positioning brings an important advantage over the ion current feedback when working in diluted electrolytes. Unlike in SICM, the positioning capabilities of the FluidFM remain completely unaffected by the noisier currents observed when approaching substrates in 1 mM KCl (see in Figure 2c compared to the measurements in 10 mM): since the amplitude of the current reduces upon dilution, accurate landing of the probe in SICM methods becomes more difficult as the feedback relies on the noisier and smaller current magnitudes; on the contrary, the FluidFM enables imaging using feedback based on force detection (AFM contact mode), where the noise level stays independent of the electrolyte concentration. Therefore, we can take full advantage of the increased surface charge sensitivity of the FluidFM nanopipette when working at low electrolyte concentrations without an associated loss in topographical resolution thanks to the AFM control.

Figure 3 shows the contrast enhancement offered by working at lower concentrations when imaging a partial polystyrene film covering a glass substrate. The uncharged polystyrene layer forms a thin film with some areas exposing directly the underlying negatively charged glass coverslip, representing a sample with a combination of spatially distributed topographical and charge features. The AFM topography and simultaneous current maps of this substrate were acquired in 10 mM (Figure 3a and b) and 1 mM (Figure 3c and d). Since in this work glass was chosen as the common substrate for both the PDL and polystyrene samples the current is normalized to its magnitude in contact with the glass for easier comparison between these sets of experiments. Figure 3a shows the topography of the partial polystyrene film with clearly resolved circular features that correspond to the defects in the polystyrene film, where the underlying glass substrate is exposed. The simultaneous normalized current map (Figure 3b), recorded at negative bias, shows a clear difference between the two materials, as the uncharged polystyrene appears darker (lower current) than the negatively charged glass due to the difference in SIR on these materials. Importantly, some local variations of charge do not correlate to identifiable changes in topography (a few examples are pointed out by the light-grey arrows), highlighting the independent nature of topographical and charge sensing.

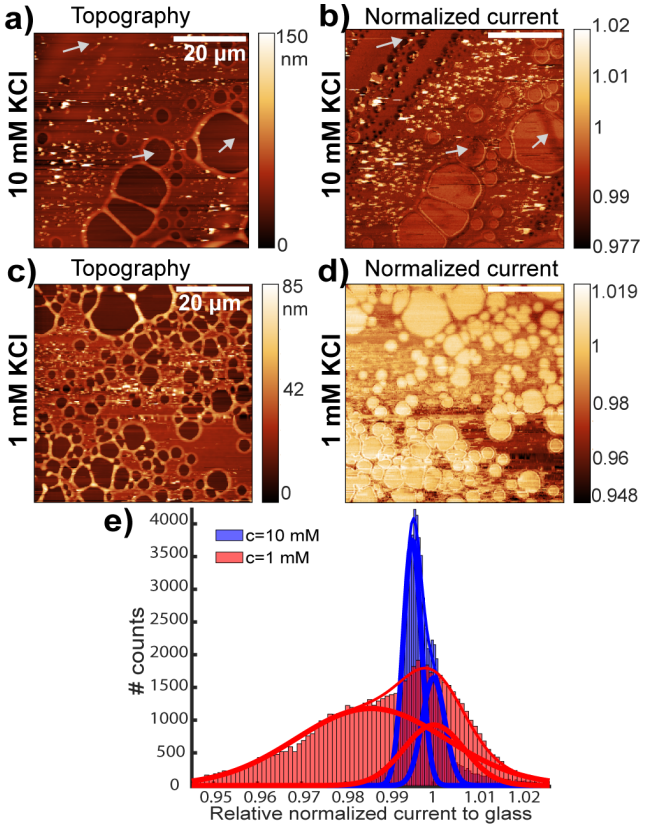

Figure 3. Simultaneous topographical and ion current imaging in 10 mM KCl (a, b) and 1 mM KCl (c, d) of a partial polystyrene film on glass (solutions pH = 6.2) acquired under same imaging conditions (bias -0.7 V, SP 5 nN, 3 s/line). The current is normalized to the current on the glass at contact. The grey arrows in (a) and (b) show current variations not associated with topography (more detailed comparison is shown in Supporting Information SI-4). e) Histograms of the current images in 10 mM KCl (blue), and 1 mM KCl (red) with their Gaussian fits (thin lines), resulting from the summation of two individual Gaussian distributions (thicker lines).

As discussed above, lowering the electrolyte concentration has a strong effect in the ion current contrast observed during imaging. Figure 3c and d display topography and ion current as measured over another area on the polystyrene sample at the lower electrolyte concentration of 1 mM. A clear contrast enhancement as compared to imaging in 10 mM KCl is

observed: while the topography exhibits similar features, a larger difference in current magnitudes enables more evident distinction between the materials. This is further emphasized in Figure 3e that shows the histogram of the recorded current magnitudes in both electrolytes (1 mM and 10 mM) where two peaks associated with the probe current on glass and on polystyrene can be identified. For further analysis of the current values on the respective images we fitted the histograms (thin lines in Figure 3e) assuming those to be formed by two Gaussians (thick lines in Figure 3e, fitting details in the Supporting Information SI-5). In 10 mM KCl (blue lines) this examination enables identification of two peaks: the distinct peak centered around 1 is attributed to the imaging on glass (due to current normalization by definition herein), while the other peak, more intense, is centered at 0.995 (*i.e.* 0.5 % difference to glass) and corresponds to the uncharged polystyrene. Peak intensities (to be precise, the areas under the peaks) determine the surface coverage by both materials, as observed on the image.

Analysis of the intensities read out in 1 mM KCl is also represented in a form of a histogram and is shown in Figure 3e (red lines). A closer examination of each distribution enables to identify two Gaussians: one at 1 (glass) and another at 0.985 (polystyrene), therefore displaying a higher current contrast compared to the 10 mM KCl (1.5 % difference *vs.* 0.5 %, respectively). These distributions also exhibit broader standard deviations, that is 17.0 x 10^{-3} and 6.8 x 10^{-3} for 1 mM *vs.* 2.0 x 10^{-3} and 2.6 x 10^{-3} for 10 mM, on polystyrene and glass, respectively. This highlights the wider range of surface charge magnitudes which can be probed and distinguished with the FluidFM in diluted electrolytes on the relatively large scanned area (60 µm by 60 µm). Even though the definite reason for this variation of the measured charge remains unclear, it is likely to be attributed to small defects (holes) in the polystyrene film contributing to SIR[21] and potential electrostatic charging (for instance, due to triboelectric effects) which can take place on both glass and polymer layers.[34,35]

High-speed imaging

Electrochemical scanning probe methods, despite recent improvements,[36–39] suffer from slow image acquisition rates. Regardless the efficiency of nanopipette approaches for local sensing,[39] state-of-the-art techniques for charge mapping are among the slowest imaging methods since their imaging speed has significantly suffered from the need to decorrelate charge and topography, which are both read-out using the probe ion current. Until now the only methods that could successfully resolve simultaneously topography and charge distribution required to use hopping mode.[14,15,20,21] In this procedure[40] the probe is approached to the sample at every image pixel for which the topography is firstly probed, by operating under reduced bias to minimize charge contribution[14,21] or by using feedback on the phase shift in the bias modulation mode.[20] Then the charges are extracted from the current recorded during a potential sweep[15,20] or pulse[21] at each pixel. This step constitutes the bottleneck of those charge-mapping strategies, as at each position the current response from the potential sweep/pulse needs to be compared to the same measurement in bulk to properly estimate the magnitude of the SIR. This results in imaging speeds that require at least 100 ms per pixel,[21] therefore demanding a compromise between image quality (number of pixels per unit area), image size and acquisition time (typically ranging from tens of minutes to several hours). Other strategies[16] also employ ion current through a nanopipette for charge imaging but do not offer a simultaneous topographical information about the scanned area. Instead, charge information is extracted from comparing two SICM images acquired by raster scanning the probe at two opposite biases. The improved scan rate of this protocol (usually around 10 ms per pixel, as a result of a scan frequency of 0.3 Hz and the necessity to scan twice the same area at opposite biases) then gets challenged by the need to perform a complementary AFM imaging for topography characterization, which introduces additional experimental difficulties associated with the need to sequentially image the exact same sample area.

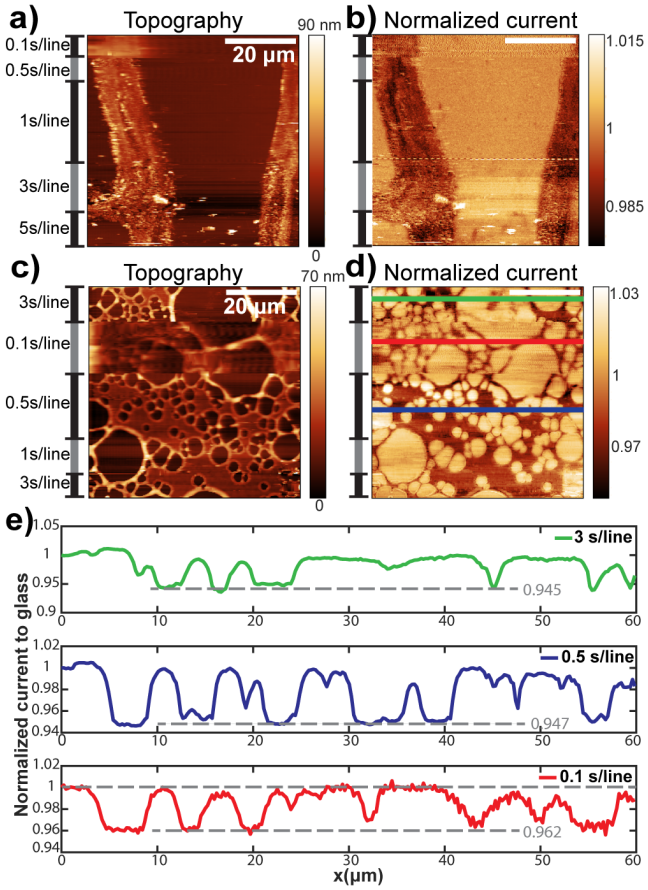

Figure 4. High speed topographical and simultaneous current imaging of a,b) a microcontact printed PDL sample (pH=5.6) and c,d) a polystyrene sample (pH=6.2). Both images were acquired in AFM contact mode (SP 5 nN, bias - 0.7 V) at varying scanning speeds indicated on the side of the topography images. The current is normalized to the current amplitude on the glass in contact. The colored lines of (d) show the position of the different line profiles depicted in (e). Please refer to Supporting Information SI-6 to see the patterned PDL area imaged in (a).

In this work, we take advantage of the independent ion current measurements and force-controlled vertical probe feedback to perform simultaneous high-speed imaging by raster scanning the probe instead of hopping. AFM force feedback is one of the most robust and reliable methods for vertical probe positioning in scanning probe methods, enabling scanning of a wide range of materials from individual biomolecules to living cells and hard interfaces,[41] while allowing fast imaging with rates up to 1300 frames per second.[42] Figures 4a and c depict the topography of both a delicate (PDL) and hard (polystyrene) thin film on glass, recorded with FluidFM cantilevers in contact

AFM mode at variable scan rates. As can be seen, these topographical maps show negligible differences in image quality when resolving surface features at scans of 5 – 0.5 s per image line (corresponding scan rates of 0.1 and 1 Hz). Topographies of both surface "pits" (defects in polystyrene film) and "hills" (PDL deposits) are well resolved with scan rates up to 0.1 s per line (5 Hz), where the topographical maps start to blur due to inaccurate tracking of the surface topography at high probe translation rates (in this case reaching 600 μm s^{-1}). After decreasing the scan rate back to 3 s per line, *i.e.* 20 μm s^{-1} (see the top part of Figure 4c), the performance of the AFM controller is restored and the topography is again well resolved.

Interestingly, the corresponding simultaneous ion current maps (Figures 4b and d) recorded during AFM imaging show notably less distortion (as compared to topographical images in Figure 4a and c) even at high probe translation rates. Both images of the PDL and polystyrene demonstrate clear contrast for all the investigated scan speeds, depicting an evident distinction between materials bearing positive (PDL) or neutral (polystyrene) surface charges and the negatively charged glass. Comparison between the topographical and ion current maps also demonstrates that substrate topography does not affect electrical measurements: small topographical details on the edges of the PDL patterns (Figure 4a) and increased heights around the defects of polystyrene film (Figure 4c) cannot be found on the corresponding current images (Figures 4b and d). Importantly, we also did not find evidence of orifice clogging or contamination (due to substrate scratching) during scanning, even on soft and relatively weakly adhered layers, such as PDL.

Even though ion current maps are significantly less affected by scanning at high frame rates than their corresponding topographical images, a particular care has to be taken whenever quantitative analysis of the measured current rectification at the interface is required. Detailed analysis of the recorded ion current at various translation rates is shown in Figure 4e, depicting the current line profiles of the polystyrene sample recorded at speeds of 3 s, 0.5 s and 0.1 s scanning time per line (see corresponding topography profiles in Supporting Information SI-7). For the first two cases (3 and 0.5 s per line, equivalent to 11.7 and 2 ms per image pixel respectively), normalized current magnitudes vary between 1 on glass and 0.945 on polystyrene, therefore determining an overall 5.5 % difference in current between the two materials of different charge. However, the increase of speed to 0.1 s per line (0.4 ms per image pixel) causes a slight reduction of the current contrast, with current magnitudes varying between 1 and 0.962 (*i.e.* 3.8 % difference in current), indicating a drop of rectification factor induced by the EDL at the interface. This can be related to several factors. First of all, to the change of the tip-to-substrate distance due to a relatively slow response of our AFM feedback control at high translation rates evident from the topographical images of Figure 4a and c and the higher noise level in Figure 4e. Secondly, at 0.1 s per line, the scan rate becomes comparable to the rate of ion redistribution characteristic to the ion current rectification phenomenon. A typical timescale for ion accumulation or depletion (that determine current contrast for charge mapping) in conical nanopores and nanopipettes is usually within 1 – 10 ms.[14,33] For the probe translated at 120 μm s^{-1} (0.5 s per line), the probe residence time over a scanned area corresponding to the size of the probe opening (300 nm in our case) is 2.5 ms, which is still within the time required for complete accumulation/depletion and does not lead to noticeable loss in contrast (no delay in ion transport). On the other hand, for the probe scanned at 600 μm s^{-1} (0.1 s per line), the probe residence time is only 0.5 ms, clearly insufficient to reach complete high/low current states of the ICR. Even though for qualitative imaging a slight drop of imaging contrast might not become an issue, our results show that protocols that would attempt to quantitatively estimate surface charge magnitudes with steady-state numerical simulation of ion fluxes through the pipette (*i.e.* ignoring time-dependent phenomena) can almost certainly lead to incorrect interpretation of experimental data at those high scanning rates. Therefore, a physical limit of scanning speed for quantitative surface charge mapping is given by the ratio of the probe size over the translation rate, which should not fall short of the characteristic times of ion redistribution (1-10 ms). In our case, we experimentally confirmed this limit to be around 120 μm s^{-1} for a typical FluidFM cantilever, equating to a 2.5 ms residence time or a scan speed of 0.5 s per line when considering imaging conditions as in Figure 4, as only a limited sign of loss in contrast can be identified in this case (less than 0.2 %). This speed corresponds to a 2 ms per pixel acquisition rate, which is two orders of magnitude faster than previously reported approaches for surface charge mapping.

CONCLUSION

We report here an advanced approach for mapping local rectifying behavior at interfaces relevant to the presence of uncompensated surface charge using a microfabricated FluidFM nanopipette. This microchanneled cantilever with a 300 nm opening combines robust and versatile capabilities of the atomic force microscope with the principles of probing local ionic environment of the electrical double layer existing at the substrate. The simultaneous measurement of ion current through the probe orifice along with the force detection enable accurate probe positioning for topographical scanning and entirely independent charge mapping. This provides a high sensitivity to this approach from the possibility of working in diluted electrolyte solutions, where the rectification and surface charge effects are amplified, but where ion current-based positioning as currently used for charge mapping with nanopipettes can become troublesome. Furthermore, the FluidFM enables a significant imaging speed increase overtaking the existing methods by two orders of magnitude (the probes reach translation rates of 120 μm s^{-1} equating to 2 ms per pixel) and reaches the physical speed limit of rectification-based surface charge imaging.

Further advancements of our approach are on the way. Although in this work commercially available cantilevers with opening diameters of 300 nm were employed, a decrease of the probe size can be readily achieved (with the use of advanced microfabrication techniques, *e.g.* focused ion beam milling), while there is a high chance that microfabricated probes with smaller apertures will hit the market in the near future. This will open up opportunities for mapping charges on living cells and tissues under physiological conditions (high ionic strength, where the current FluidFM nanopipettes have limited sensitivity towards SIR). This would probably require non-contact or intermittent-contact AFM feedback for probe positioning in order to avoid damage in such biological systems. Also, further quantitative analysis of the rectifying behavior at interfaces during scanning with FluidFM probes can be performed with the help of finite element method simulations. Even though this remains overlooked in this work (mainly due

to a relative complexity of calculations coming from the probe geometry that requires a three-dimensional simulation), mathematical analysis of ion currents in FluidFM configuration will enable quantification of surface charge. Furthermore, we expect a wider use of this methodology for probing charges on a variety of materials (*e.g.* crystals, minerals), where it might be convenient to use organic solvents (ionic strength is typically low due to poor dissociation of salts) and where our approach would naturally excel over other methods.

ASSOCIATED CONTENT

Supporting Information

The Supporting Information is available free of charge on the ACS Publications website.

Characterization of the FluidFM probes (geometry, working distance and electrical properties), imaging results at positive probe biases, measurement reproducibility, zoomed views on topography and ion current images in 10 mM KCl, details on histograms fitting, fluorescent image of the PDL sample, AFM topography profiles (PDF).

AUTHOR INFORMATION

Corresponding Author

* momotenko@biomed.ee.ethz.ch

Notes

The authors declare no competing financial interests.

ACKNOWLEDGMENT

The work was supported by the Swiss National Science Foundation Ambizione Grant PZ00P2_174217/1 (D.M.) and the EUROSTARS project grant E!11644 (T.Z.). The authors also acknowledge Edin Sarajlic (SmartTip BV, Netherlands), Patrick Frederix (Nanosurf AG, Switzerland), Pablo Dörig, Alexander Serre and Dario Ossola (all Cytosurge AG, Switzerland) for their kind support as well as Stephen Wheeler (ETH Zurich) for technical assistance. The authors also acknowledge Dr. Maria Adobes Vidal (ETH Zurich) for fruitful scientific discussions.

REFERENCES

(1) Trefalt, G.; Behrens, S. H.; Borkovec, M. *Langmuir* **2016**, *32*, 380–400.
(2) Ayala, V.; Herrera, A. P.; Latorre-Esteves, M.; Torres-Lugo, M.; Rinaldi, C. *J. Nanopart. Res.* **2013**, *15*, 1874.
(3) Oncsik, T.; Trefalt, G.; Csendes, Z.; Szilagyi, I.; Borkovec, M. *Langmuir* **2014**, *30*, 733–741.
(4) Fröhlich, E. *Int. J. Nanomed.* **2012**, *7*, 5577–5591.
(5) Ghosh, P. S.; Kim, C.; Han, G.; Forbes, N. S.; Rotello, V. M. *ACS Nano* **2008**, *2*, 2213–2218.
(6) Sprycha, R. *J. Colloid Interface Sci.* **1989**, *127*, 1–11.
(7) Lützenkirchen, J.; Preočanin, T.; Kovačević, D.; Tomišić, V.; Lövgren, L.; Kallay, N. *Croat. Chem. Acta* **2012**, *85*, 391–417.
(8) Hillier, A. C.; Kim, S.; Bard, A. J. *J. Phys. Chem.* **1996**, *3654*, 18808–18817.
(9) Miyatani, T.; Horii, M.; Rosa, A.; Fujihira, M.; Marti, O. *Appl. Phys. Lett.* **1997**, *71* (18), 2632–2634.
(10) Ahimou, F.; Denis, F. A.; Touhami, A.; Dufrene, Y. F. *Langmuir* **2002**, *18*, 9937–9941.
(11) Almonte, L.; Lopez-Elvira, E.; Baro, A. M. *ChemPhysChem* **2014**, *15*, 2768–2773.
(12) Sotres, J.; Baró, A. M. *Biophys. J.* **2010**, *98*, 1995–2004.
(13) Hansma, P. K.; Drake, B.; Marti, O.; Gould, S. A. .; Prater, C. . *Science* **1989**, *243*, 641–643.
(14) Mckelvey, K.; Kinnear, S. L.; Perry, D.; Momotenko, D.; Unwin, P. R. *J. Am. Chem. Soc.* **2014**, *136*, 13735–13744.
(15) Perry, D.; Paulose Nadappuram, B.; Momotenko, D.; Voyias, P. D.; Page, A.; Tripathi, G.; Frenguelli, B. G.; Unwin, P. R. *J. Am. Chem. Soc.* **2016**, *138*, 3152–3160.
(16) Klausen, L. H.; Fuhs, T.; Dong, M. *Nat. Commun.* **2016**, *7*, 12447.
(17) Ossola, D.; Dorwling-Carter, L.; Dermutz, H.; Behr, P.; Vörös, J.; Zambelli, T. *Phys. Rev. Lett.* **2015**, *115*, 238103.
(18) Page, A.; Perry, D.; Unwin, P. R. *Proc. R. Soc. A* **2017**, *473*, 20160889.
(19) Korchev, Y. E.; Bashford, C. L.; Milovanovic, M.; Vodyanoy, I. *Biophys. J.* **1997**, *73*, 653–658.
(20) Perry, D.; Al Botros, R.; Momotenko, D.; Kinnear, S. L.; Unwin, P. R. *ACS Nano* **2015**, *9*, 7266–7276.
(21) Page, A.; Perry, D.; Young, P.; Mitchell, D.; Frenguelli, B. G.; Unwin, P. R. *Anal. Chem.* **2016**, *88*, 10854–10859.
(22) Fuhs, T.; Klausen, L. H.; Sønderskov, S. M.; Han, X.; Dong, M. *Nanoscale* **2018**, *10*, 4538–4544.
(23) Sa, N.; Baker, L. A. *J. Am. Chem. Soc.* **2011**, *133*, 10398–10401.
(24) Sa, N.; Lan, W. J.; Shi, W.; Baker, L. A. *ACS Nano* **2013**, *7*, 11272–11282.
(25) Wei, C.; Bard, A. J.; Feldberg, S. W. *Anal. Chem.* **1997**, *69*, 4627–4633.
(26) Meister, A.; Gabi, M.; Behr, P.; Studer, P.; Vörös, J.; Niedermann, P.; Bitterli, J.; Polesel-Maris, J.; Liley, M.; Heinzelmann, H.; et al. *Nano Lett.* **2009**, *9*, 2501–2507.
(27) Ricoult, S. G.; Goldman, J. S.; Stellwagen, D.; Juncker, D.; Kennedy, T. E. *J. Neurosci. Methods* **2012**, *208*, 10–17.
(28) Guillaume-Gentil, O.; Potthoff, E.; Ossola, D.; Franz, C. M.; Zambelli, T.; Vorholt, J. *Trends Biotechnol.* **2014**, *32*, 381–388.
(29) Ossola, D.; Amarouch, M.-Y.; Behr, P.; Vörös, J.; Abriel, H.; Zambelli, T. *Nano Lett.* **2015**, *15*, 1743–1750.
(30) Perry, D.; Momotenko, D.; Lazenby, R. A.; Kang, M.; Unwin, P. R. *Anal. Chem.* **2016**, *88*, 5523–5530.
(31) Xu, S.; Arnsdorf, M. *Proc. Natl. Acad. Sci. USA* **1995**, *92*, 10384–10388.
(32) White, H. S.; Bund, A. *Langmuir* **2008**, *24*, 2212–2218.
(33) Guerrette, J. P.; Zhang, B. *J. Am. Chem. Soc.* **2010**, *132*, 17088.
(34) Lacks, D. J. *Angew. Chem. , Int. Ed.* **2012**, *51*, 6822–6823.
(35) Baytekin, H. T.; Patashinski, A. Z.; Branicki, M.; Baytekin, B.; Soh, S.; Grzybowski, B. A. *Science* **2011**, *333*, 308–312.
(36) Ida, H.; Takahashi, Y.; Kumatani, A.; Shiku, H.; Matsue, T. *Anal. Chem.* **2017**, *89*, 6015–6020.
(37) Novak, P.; Shevchuk, A.; Ruenraroengsak, P.; Miragoli, M.; Thorley, A. J.; Klenerman, D.; Tetley, T. D.; Gorelik, J.; Korchev, Y. E. *Nano Lett.* **2014**, *14*, 1202–1207.
(38) Momotenko, D.; Byers, J. C.; McKelvey, K.; Kang, M.; Unwin, P. R. *ACS Nano* **2015**, *9*, 8942–8952.
(39) Momotenko, D.; Mckelvey, K.; Kang, M.; Meloni, G. N.; Unwin, P. R. *Anal. Chem.* **2016**, *88*, 2838–2846.
(40) Novak, P.; Li, C.; Shevchuk, A. I.; Stepanyan, R.; Caldwell, M.; Hughes, S.; Smart, T. G.; Gorelik, J.; Ostanin, V. P.; Moss, G. W. J.; et al. *Nat. Methods* **2009**, *6*, 279–282.
(41) Dufrêne, Y. F.; Ando, T.; Garcia, R.; Alsteens, D.; Martinez-Martin, D.; Engel, A.; Gerber, C.; Müller, D. J. *Nat. Nanotechnol.* **2017**, *12*, 295–307.
(42) Picco, L. M.; Bozec, L.; Ulcinas, A.; Engledew, D. J.; Antognozzi, M.; Horton, M. A.; Miles, M. J. *Nanotechnology* **2007**, *18*, 044030.

For TOC only

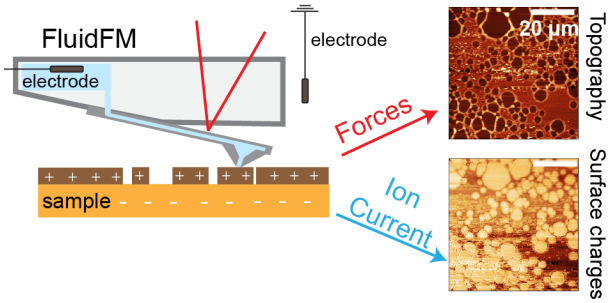
FluidFM
electrode
electrode
sample
Forces
Ion
Current
20 µm
Topography
Surface charges